Transpiration Nosetip Coolant Flow Control

JOHN R. SCHUSTER,* ROGER A. GLICKMAN,† AND DOUGLAS R. HENDER‡
McDonnell Douglas Astronautics Co., Huntington Beach, Calif.

The coolant requirements of transpiration nosetips are determined through use of detailed computer analyses of the flowfield, aerodynamic heating, and porous matrix coolant flow. Utilizing the detailed results, curve fits are established for boundary-layer parameters in terms of freestream velocity and density, and simplified heat-transfer and coolant flow-control equations are developed. The maximum net coolant wastage using the flow-control equation for a family of five advanced trajectories having stagnation pressures up to 244 atm and angles of attack up to 26° is only 11.9%. In conjunction with the development of the flow-control equation, simple relationships are derived to yield velocity, density, and angle of attack from vehicle axial and lateral accelerations.

Nomenclature

A_B = vehicle base area, ft^2
C = vehicle drag coefficient, dimensionless
C_p = specific heat, Btu/lbm-°R
C_1, C_2, C_3 = constants defined by Eq. (42), dimensionless
C_4 = constant defined by Eq. (48), dimensionless
C_5 = constant defined by Eq. (48), ft^{-1}
C_6 = constant defined by Eq. (48), ft^{-2}
C_7 = constant defined by Eq. (48), ft^{-3}
f = function, dimensionless
g_c = conversion factor, 32.17 lbm-ft/lbf-sec^2
H = enthalpy, Btu/lbm
h = geometric altitude, ft
J = conversion factor, 778 lbf-ft/Btu
K = ratio between nosetip inner surface pressure and stagnation pressure, dimensionless
k = porous matrix permeability, ft^2
K_1 = constant defined by Eq. (31), lbm$^{1-K_2}$ ft$^{3K_2-K_3}$ sec$^{K_3-1}$
K_2, K_3 = constants defined by Eq. (31), dimensionless
K_4 = constant defined by Eq. (38), dimensionless
K_5, K_6, K_7 = constants defined by Eq. (39), dimensionless
M = vehicle mass, lbm
$\dot{m}$ = coolant flux, lbm/ft^2-sec
N = heat transfer coefficient, lbm/ft^2-sec
P = pressure, lbf/ft^2
Pr = Prandtl number, dimensionless
q = dynamic pressure, lbf/ft^2
$\dot{q}$ = heat flux, Btu/ft^2-sec
R = radius measured to nosetip axis of symmetry, ft
r = recovery factor, dimensionless
Re = Reynolds number, dimensionless
T = temperature, °R
t = time, sec
u = velocity, fps
$\dot{w}$ = coolant flow rate, lbm/sec
α = angle of attack, radians
β = porous matrix inertial pressure-drop constant, ft^{-1}
ε = effective emissivity of surface, dimensionless
η = vehicle acceleration, ft/sec^2
θ = included angle between nosetip axis of symmetry and surface normal, radians
μ = viscosity, lbm/ft-sec
ξ_N = ratio of normal to axial acceleration, dimensionless
ρ = density, lbm/ft^3
σ = Stefan-Boltzmann constant, 0.476×10^{-12} Btu/ft^2-sec-°R^4
Φ = surface integral defined by Eq. (22), dimensionless

Superscript
* = effective value with blowing

Subscripts
a, b = evaluated at Time Points a and b, respectively
c = convective
D = drag component parallel to freestream vector
e = boundary-layer edge
i = nosetip inner surface
L = lift component perpendicular to freestream vector
N = normal to vehicle axis
n = nosetip
o = stagnation
r = recovery
ref = reference value
s = nosetip outer surface
sink = sink for thermal radiation
v = value for coolant vapor phase
x, y = in vehicle yaw and pitch plane, respectively
Z = along vehicle axis
α = evaluated at an angle-of-attack α
θ = evaluated at angle θ from the stagnation point
∞ = freestream
34 = evaluated at an angle of 34° from the stagnation point

Presented as Paper 73-767 at the AIAA 8th Thermophysics Conference, Palm Springs, Calif., July 16–18, 1973; submitted July 23, 1973; revision received November 2, 1973. This work was supported by USAF Contract F04701-72-C-0233 under the direction of Capt. M. L. Anderson of the Space and Missile Systems Organization and R. W. Young of the Aerospace Corporation.

Index categories: LV/M Aerodynamic Heating; Boundary Layers and Convective Heat Transfer—Turbulent; Viscous Nonboundary-Layer Flows.

* Senior Engineer Scientist, Aerothermodynamics.
† Engineer Scientist Specialist, Saturn Mechanical.
‡ Engineer Scientist Specialist, Aerothermodynamics.

Introduction

TRANSPIRATION cooling represents the only practical design solution for advanced aerodynamic vehicles that require nosetips with stable shapes. Cooling by this method appears to have no upper heating-rate limitation. Recently, the weight and volume of the coolant storage and expulsion system have been regarded as a major area where design improvements can be made. Some of the studies have been devoted to defining a flow-control approach that can closely match the time-varying coolant requirements of the vehicle nosetip and also be responsive to off-nominal heating conditions. One promising concept for flow control employs an electromechanical valve driven with a signal derived from vehicle aerodynamic parameters. This paper describes the development of a flow-control analog in equation form that utilizes vehicle parameters and provides excellent correlation with required coolant flow.

Analysis

The basic approach generally used to analyze transpiration cooling is to decouple the porous matrix flow and boundary-layer flow. This is done by assuming surface-temperature distri-

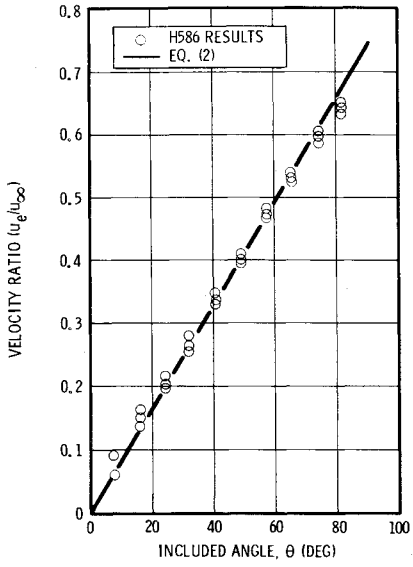

Fig. 1 Ratio of local to freestream velocity.

butions and boundary-layer similarity such that thermally ideal coolant flux distributions can be evaluated for the heated surface. The porous matrix is then designed such that its hydraulic characteristics result in an actual coolant distribution that closely matches the thermally ideal distribution. In practice, the aerodynamic heating is readily determined by use of complex computer programs that utilize atmospheric tables, tables of real-gas properties, and shock-wave relationships to provide boundary-layer edge properties. In addition, porous matrix coolant flow is analyzed with three-dimensional, finite-difference methods to account for varying coolant properties, tangential pressure gradients, and both viscous and inertial flow characteristics of the coolant in the microscopic structure. Some of the development done in this paper relies on the results of computer programs H586[1] and H859,[2] which enploy such detail. The accuracy of their calculations is assumed in all future analytical developments.

Nosetip Boundary Layer

Because of uncertainty about the effect of transpiration on boundary-layer transition, current practice is to assume that turbulence begins a short distance downstream of the stagnation point. In essence, transpiration nosetip designs reflect a turbulent heating distribution such as would result from the application of Van Driest's[3] equation.

$$\dot{q}_c = (0.048/Pr^{2/3})\, Re_s^{-0.2} \rho_e u_e (H_r - H_s) \qquad (1)$$

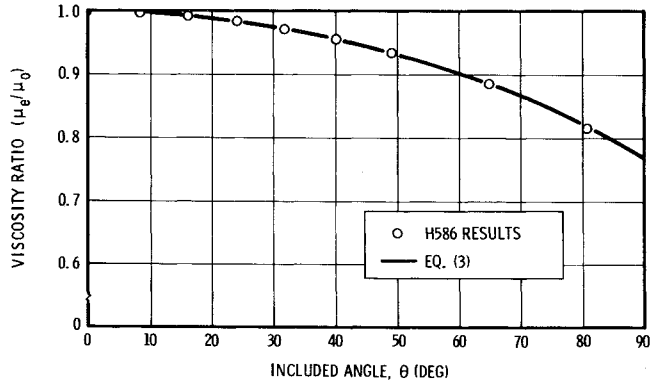

Fig. 2 Ratio of local to stagnation-point viscosity.

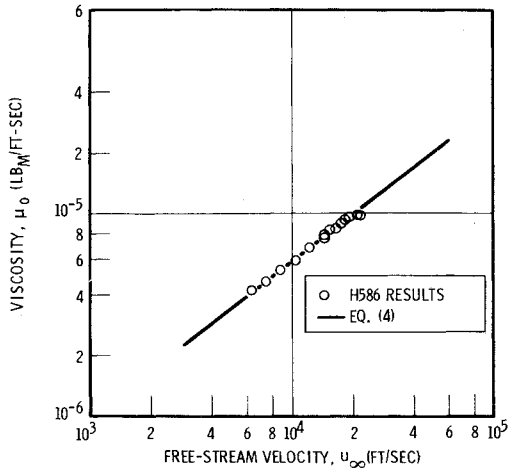

Fig. 3 Stagnation-point viscosity.

A series of re-entry turbulent heating conditions for hemispheres was analyzed and the results were correlated using basic flowfield parameters and Eq. (1).

Edge Properties

Figure 1 presents a correlation of results for the ratio u_e/u_∞, which can be correlated by the following equation:

$$\begin{aligned} u_e/u_\infty &= 0.41\theta \text{ above } 70{,}000 \text{ ft} \\ &= 0.48\theta \text{ below } 70{,}000 \text{ ft} \end{aligned} \qquad (2)$$

where θ is the local angle to the stagnation point. The local boundary-layer edge viscosity is shown in Fig. 2 and is correlated on the basis of stagnation-point viscosity by Eq. (3)

$$\mu_e/\mu_0 = (1.0 - 0.168\theta^2)^{0.5} \qquad (3)$$

while the stagnation viscosity is presented in Fig. 3 and is correlated by Eq. (4).

$$\mu_0 = 5.0 \times 10^{-8} u_\infty^{0.767} \qquad (4)$$

Figure 4 presents the results of two correlation methods for predicting local pressure. The popular cosine-squared distribution leaves much to be desired, while the power law expression in Eq. (5) matches the H586 results well.

$$P_e/P_0 = 0.275^{\theta 2} \qquad (5)$$

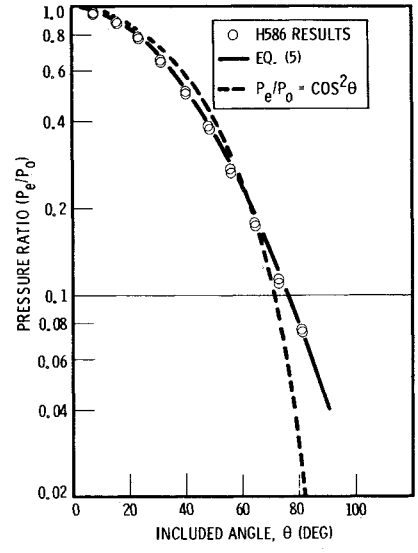

Fig. 4 Local surface pressure.

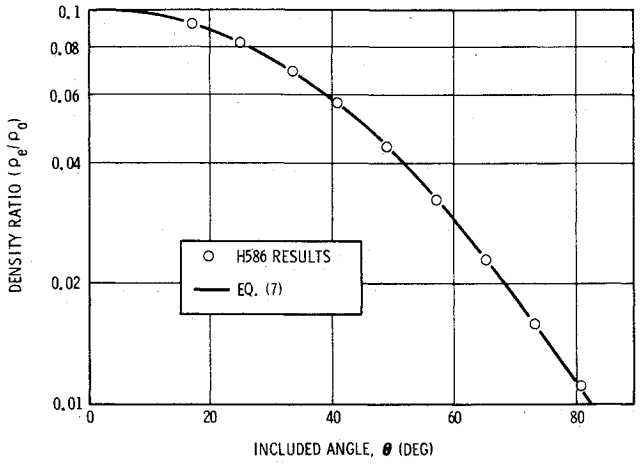

Fig. 5 Ratio of local to stagnation-point density.

Making the assumption that

$$\frac{\rho_e}{\rho_o} = \frac{P_e/P_o}{f(H_e/H_o)} \tag{6}$$

the boundary-layer edge density is found to be correlated by Eq. (7) and appears in Fig. 5.

$$\frac{\rho_e}{\rho_o} = \frac{0.275^{\theta^2}}{(1.0-0.168\theta^2)} \tag{7}$$

The curve of freestream to stagnation-point density ratio is shown in Fig. 6 and is approximated well by Eq. (8) in the range of freestream velocity from 7000 fps to 20,000 fps.

$$\frac{\rho_\infty}{\rho_o} = 6.05u_\infty{}^{-0.424} \tag{8}$$

Making the necessary substitutions, the boundary-layer edge properties in terms of freestream density, velocity, and local slope are:

edge velocity

$$\begin{aligned} u_e &= 0.41\theta u_\infty \text{ above } 70{,}000 \text{ ft} \\ &= 0.48\theta u_\infty \text{ below } 70{,}000 \text{ ft} \end{aligned} \tag{9}$$

edge viscosity

$$\mu_e = 5.0\times10^{-8}u_\infty{}^{0.767}\times(1.0-0.168\theta^2)^{0.5} \tag{10}$$

edge pressure

$$P_e = 0.92(0.275^{\theta^2})\rho_\infty u_\infty{}^2 \tag{11}$$

edge enthalpy

$$H_e = 2.0\times10^{-5}u_\infty{}^2\times(1.0-0.168\theta^2) \tag{12}$$

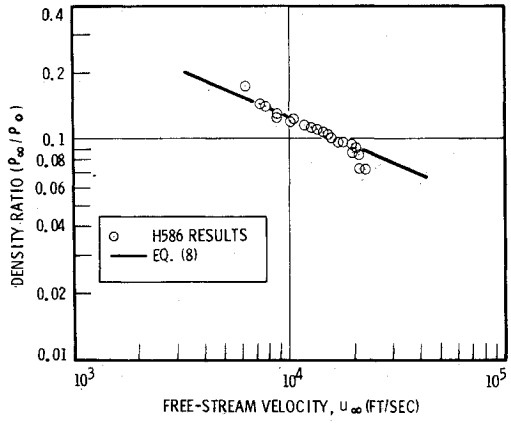

Fig. 6 Ratio of freestream to stagnation-point density.

edge density

$$\rho_e = 0.165\rho_\infty u_\infty{}^{0.424}\times(0.275^{\theta^2})/(1.0-0.168\theta^2) \tag{13}$$

Heating

Making the necessary substitutions, a local enthalpy heat transfer coefficient may be defined based on Eq. (1) and is found to be

$$N_c = \frac{2.18\times10^{-4}\rho_\infty{}^{0.8}u_\infty{}^{1.29}}{Pr^{2/3}R_n{}^{0.2}}\,\frac{\theta^{0.6}(0.275)^{0.8\theta^2}}{(1.0-0.168\theta^2)^{0.7}} \tag{14}$$

Approximating the enthalpy potential for heat transfer as the kinetic enthalpy, Eq. (1) becomes

$$\dot{q}_c = 5.53\times10^{-9}\,\frac{\rho_\infty{}^{0.8}u_\infty{}^{3.29}}{R_n{}^{0.2}}\,\frac{\theta^{0.6}(0.275)^{0.8\theta^2}}{(1.0-0.168\theta^2)^{0.7}} \tag{15}$$

with the maximum heat flux occurring approximately 34° from the stagnation point.

Boundary-Layer Mass Transfer Effects

For a transpired boundary layer, a surface-energy balance yields the following equation:

$$\dot{q}_c = \frac{\varepsilon\sigma(T_s^4 - T_{\text{sink}}^4)+\dot{m}\Delta H}{N_c{}^*/N_c} \tag{16}$$

where $\dot{q}_c$ is the surface convective heat flux without mass transfer; $\dot{m}$ is the thermally ideal coolant mass flux; ΔH is the net enthalpy rise of the coolant, including subcooling, heat of vaporization, and surface superheat; and $N_c{}^*/N_c$ represents the apparent reduction in heat transfer coefficient due to the mass-transfer "blocking" occurring in the boundary layer.

For relatively low surface temperature, such as would occur with liquid transpiration cooling, the radiation terms of Eq. (16) can be neglected. Expressing the heat flux in terms of the recovery enthalpy and aerodynamic heat transfer coefficient, Eq. (16) can be rearranged to

$$\dot{m}/N_c = (H_r/\Delta H)(N_c{}^*/N_c) \tag{17}$$

Bartle and Leadon,[4] Rubesin,[5] and Arne[6] have presented design correlations, based on similarity, for the ratio $N_c{}^*/N_c$. The turbulent correlation of Arne is

$$\frac{N_c{}^*}{N_c} = \frac{\left(\frac{C_{p_v}}{C_{p_s}}\right)^{0.8}\frac{\dot{m}}{N_c}}{\left[1.0+0.25\left(\frac{C_{p_v}}{C_{p_s}}\right)^{0.8}\frac{\dot{m}}{N_c}\right]^4-1.0} \tag{18}$$

where C_{p_v}/C_{p_s} is the ratio between the coolant vapor specific heat and freestream species specific heat, evaluated at the local surface pressure and local surface temperature.

Combining Eqs. (17) and (18), the thermally ideal mass flux can be expressed as

$$\dot{m} = \frac{4N_c}{(C_{p_v}/C_{p_s})^{0.8}}\left\{\left[1.0+\frac{H_r}{\Delta H}\left(\frac{C_{p_v}}{C_{p_s}}\right)^{0.8}\right]^{1/4}-1.0\right\} \tag{19}$$

For water as a coolant operating with a liquid film on the surface, the specific heat ratio is approximately 2.0 with a coolant net enthalpy rise of 1150 Btu/lbm. Using Eq. (14) for the heat transfer coefficient and the kinetic enthalpy in place of the recovery enthalpy, the local ideal coolant flux for water at an effective angle θ from the stagnation point becomes

$$\dot{m} = \frac{5.0\times10^{-4}\rho_\infty{}^{0.8}u_\infty{}^{1.29}}{Pr^{2/3}R_n{}^{0.2}}\{[1.0+3.03\times10^{-8}u_\infty{}^2]^{1/4}-1.0\}\times \frac{\theta^{0.6}(0.275)^{0.8\theta^2}}{(1.0-0.168\theta^2)^{0.7}} \tag{20}$$

with peak ideal mass flux occurring approximately 34° from the stagnation point. For other coolants, the equivalent of Eq. (20) can be derived from Eq. (19) by inserting the appropriate specific heat and enthalpy terms.

Equation (20) can be integrated over the nosetip surface area

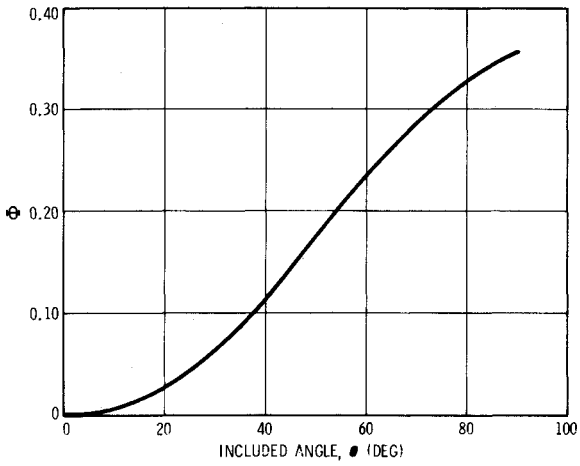

Fig. 7 Ideal coolant flux surface integral.

to obtain the thermally ideal coolant flow at zero angle of attack

$$\dot{w} = 3.16\times 10^{-3}\frac{R_n^{1.8}\rho_\infty^{0.8}u_\infty^{1.29}}{Pr^{2/3}}\times \{[1.0+3.03\times 10^{-8}u_\infty^{2}]^{1/4}-1.0\}\Phi \quad (21)$$

where

$$\Phi = \int_o^\theta \frac{\theta^{0.6}(0.275)^{0.8\theta^2}\sin\theta}{(1.0-0.168\theta^2)^{0.7}}\,d\theta \quad (22)$$

Figure 7 presents the surface integral, Φ, as a function of included angle.

Coolant Porous Flow and Nosetip Contour

In a three-dimensional porous matrix with isotropic flow properties, the modified Darcy equation can be utilized to estimate porous flow pressure gradient.

$$-g_c\nabla P = [(\mu/k)+\beta\dot{m}]\bar{\dot{m}}/\rho \quad (23)$$

The material permeability constant, k, accounts for the viscous component of the porous flow pressure drop, and the material constant, β, accounts for additional pressure drop due to inertial effects. In the micron to decamicron pore-size range, which is typical of porous nosetip material, the viscous component tends to dominate; however, the inertial component becomes more significant as coolant flux increases. To characterize the porous material, both k and β must be evaluated experimentally, as they are strongly dependent on such factors as material porosity and pore shape and size.

In order that the size of the coolant storage and expulsion system be minimized, it is desirable that there be no coolant wastage, i.e., no coolant flux in excess of that required should be delivered to any portion of the nosetip surface. It is difficult to approach this goal, particularly in view of the severe external pressure gradient that can exist. The external pressure gradient acting over the surface is transmitted into the porous material comprising the nosetip and, when superimposed on the internal radial pressure field, can cause significant bending of coolant streamlines between the nosetip inner and outer surfaces. This phenomenon, when coupled with the irregular shape of the nosetip inner surface, makes it difficult to obtain accurate estimates of coolant flow distribution.

In practice, this can be accomplished through the application of three-dimensional numerical techniques to Eq. (23), as is done in the H859 computer program. As an aid in designing the nosetip, inner contours can be established using one-dimensional analytic approximations, and then the contours can later be refined using the more comprehensive three-dimensional tools.

Seeking a local one-dimensional solution in spherical coordinates, Eq. (23) becomes

$$-g_c\frac{dP}{dR} = \left(\frac{\mu}{k\rho}+\frac{\beta\dot{m}}{\rho}\frac{R_n^2}{R^2}\right)\dot{m}\frac{R_n^2}{R^2} \quad (24)$$

where $\dot{m}$ is the coolant flux at the outer surface. Rearranging and integrating between the inner and outer surfaces

$$P_i-P_s = \frac{\mu R_n}{k\rho g_c}\left\{\frac{R_n-R_i}{R_i}\right\}\dot{m}+\frac{\beta R_n}{3\rho g_c}\left\{\frac{R_n^3-R_i^3}{R_i^3}\right\}\dot{m}^2 \quad (25)$$

If it is assumed that the heating on the hemisphere is essentially turbulent, the desired coolant distribution can be deduced from Eq. (20).

$$\dot{m}_\theta/\dot{m}_{34} = 1.88\theta^{0.6}(0.275)^{0.8\theta^2}/(1.0-0.168\theta^2)^{0.7} \quad (26)$$

From past experience, it is known that regardless of what type of contour is selected, a perfect match between ideal and actual coolant distribution cannot be achieved because of the varying stagnation pressure. The amount of coolant wastage is minimized if the nosetip permeability and contour are selected to yield a good match at the point of peak stagnation heating, which usually occurs close to the point in time of peak stagnation pressure.

Utilizing Eq. (5), and ignoring the inertial component of the porous flow pressure gradient, Eq. (25) becomes

$$\left.\frac{R_n-R_i}{R_i}\right|_\theta = \frac{P_i-0.275^{\theta^2}P_o}{(\mu R_n/k\rho g_c)\dot{m}_\theta} \quad (27)$$

If, at this design point in the trajectory, the nosetip internal pressure is related to the stagnation pressure by a factor K, i.e.,

$$P_i = KP_o \quad (28)$$

then Eqs. (26) and (27) can be combined to yield

$$\left.\frac{R_n}{R_i}\right|_\theta = 1.0+\left[\left.\frac{R_n}{R_i}\right|_{34}-1.0\right]\frac{[K-0.275^{\theta^2}][1.0-0.168\theta^2]^{0.7}}{[K-0.634][1.88\theta^{0.6}(0.275)^{0.8\theta^2}]} \quad (29)$$

The analytical contour is therefore a function of local angle, the ratio K, and the ratio between the outer and inner radii at the location of maximum heating (34°). The thinnest portion of the hemisphere occurs at the angle of maximum heating, as this is where the greatest flux of coolant is desired. The radius ratio at this angle should be chosen based on consideration of permeability, structural, and fabrication requirements. Typically this ratio has been about 1.25.

Figure 8 presents a family of nosetip inner contours generated using Eq. (29) over a range of internal-to-stagnation-pressure ratio, K. The wall thickness has been held constant below an angle of 34°.

A three-dimensional porous flow analysis of the nosetip coolant distribution was conducted using the H859 computer program. The program treats a nosetip as a nodal system, and accounts for both viscous and inertial pressure drop, angle-of-

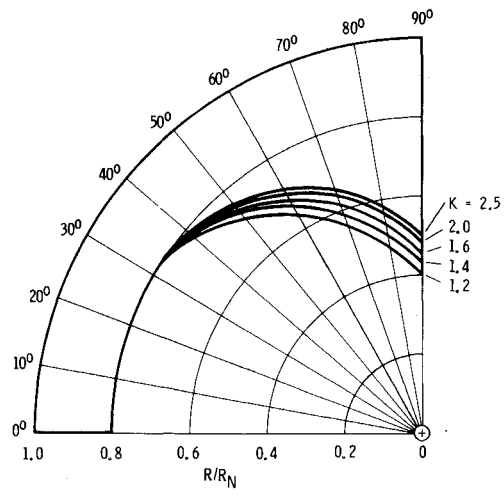

Fig. 8 Optimized nosetip contours.

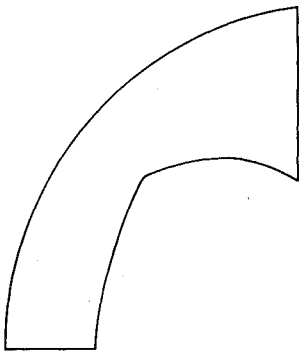

Fig. 9 Final nosetip contour.

attack effects, and viscous heating in the porous flow. Based on past experience and the desire to maintain required coolant pressure within a reasonable limit, a value of 2.0 was chosen for the ratio of coolant pressure to stagnation pressure. It was anticipated that this would also be a near-optimum value from the standpoint of coolant expulsion system weight and volume.

The ideal contours of Fig. 8 were each investigated. It was found that the best match to the ideal coolant distribution could be obtained using the contour with a value of K equal to 1.2. In addition, the contour forward of the 34° location was gradually thickened toward the stagnation point in order to reduce coolant wastage in this region. Figure 9 presents the final contour that was evolved. The design permeability of the porous material is 2.12×10^{-13} ft^2.

Angle-of-Attack Effects

Equation (21) indicates the approximate coolant flow requirement for a nosetip in terms of freestream density and velocity. If an angle of attack is imposed on the nosetip shown in Fig. 9, the thermally ideal coolant distribution required at the nosetip surface will shift with regard to the contour symmetry point, and the coolant distribution provided by the hydraulic design will no longer coincide with the ideal distribution. It is necessary to account for the effect of angle of attack on the required coolant flow. The required coolant flow provides a flux distribution at the surface that does not fall below the ideal distribution at any point on the nosetip.

For several altitude/velocity/angle-of-attack combinations, the nosetip shown in Fig. 9 was analyzed using H586, to evaluate surface pressure and ideal coolant flux distributions, and H859, to evaluate required coolant flux distributions and the associated required flow. These results were compared with the flow requirements for zero angle of attack, and the results were curve-fitted with a second-degree polynomial as shown in Fig. 10.

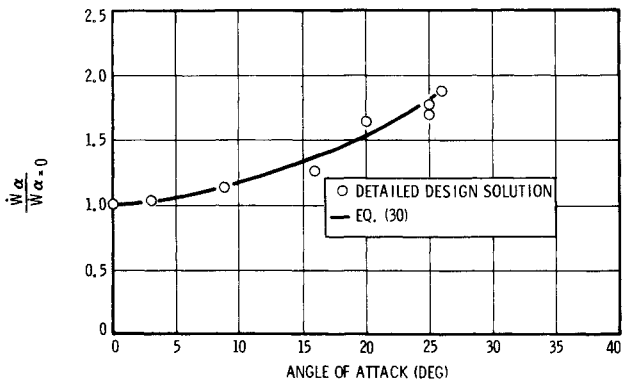

Fig. 10 Effect of angle of attack on required coolant flow rate.

$$\dot{w}_\alpha/(\dot{w}_{\alpha=0}) = 1.0+0.206|\alpha|+3.78\alpha^2 \quad (30)$$

Although Eq. (30) is restricted to the contour shown in Fig. 9, angle-of-attack effects for other contours can also be accounted for by a simple quadratic.

Final Flow-Control Equations

Although the nosetip contour shown in Fig. 9 has been optimized, the varying stagnation pressure during re-entry will significantly alter the normalized distribution of coolant at the nosetip surface. This is because of the varying stagnation pressure and the isotropic characteristics of the porous material. Assuming that a reasonable correlation exists between thermally ideal and actual distributions, Eqs. (21) and (30) suggest a flow-control equation of the form

$$\dot{w} = K_1 \rho_\infty^{K_2} u_\infty^{K_3} \{[1.0+3.03\times 10^{-8} u_\infty^2]^{1/4} - 1.0\} \times \{1.0+0.206|\alpha|+3.78\alpha^2\} \quad (31)$$

where the mass-transfer-blocking and angle-of-attack terms are retained as previously developed.

In order to determine the constants, K_1, K_2, and K_3, the set of five re-entry trajectories summarized in Table 1 was analyzed.

Table 1 Trajectory parameters

Trajectory	Re-entry velocity (fps)	Re-entry angle (deg)	Peak stagnation pressure (atm)	Peak angle of attack (deg)
1	23,400	20	110	9
2	23,400	20	51	26
3	23,500	40	244	3
4	23,500	24	54	25
5	23,600	30	93	20

For the altitude range from 125,000 ft to sea level, ideal coolant distributions and surface pressures were evaluated for a 1.0 in. radius nose using a detailed computer analysis similar to H586, and required coolant flows, with a 24% design margin, were evaluated using H859. A computer optimization was then performed to determine the three constants, resulting in Eq. (32) for the flow-control analog

$$\dot{w} = 2.86\times 10^{-4} \rho_\infty^{0.81} u_\infty^{1.0} \{[1.0+3.03\times 10^{-8} u_\infty^2]^{1/4} - 1.0\} \times \{1.0+0.206|\alpha|+3.78\alpha^2\} \quad (32)$$

Figures 11–15 present comparisons between the required coolant flows from the detailed computer analyses and the actual coolant flows from Eq. (32). The irregularities in the curves

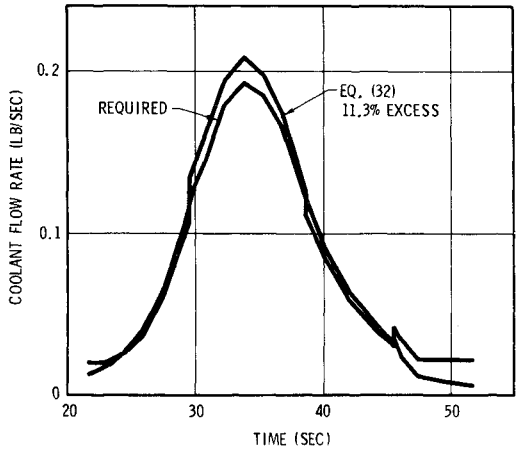

Fig. 11 Coolant flow history—Trajectory 1.

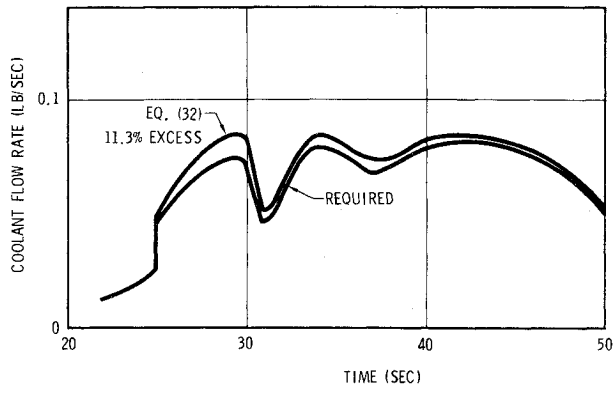

Fig. 12 Coolant flow history—Trajectory 2.

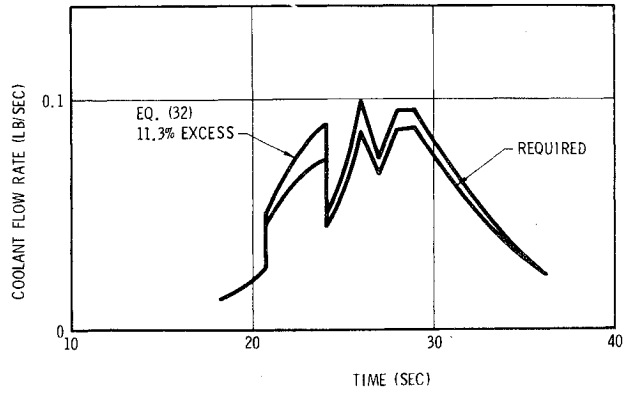

Fig. 14 Coolant flow history—Trajectory 4.

are due to varying angle of attack. For the worst-case trajectory (Fig. 15), the net coolant wastage using Eq. (32) is 11.9%. The minimum wastage of 3.75% occurs for a near-ballistic trajectory shown in Fig. 13. Close matches are obtained over essentially all portions of re-entry, and angle-of-attack effects are effectively accommodated.

For comparison, two other equations of less complexity were investigated. Equation (33) is a simple freestream density and velocity relationship with optimized coefficient and exponents

$$\dot{w} = 3.64 \times 10^{-10} \rho_\infty{}^{0.795} u_\infty{}^{2.40} \tag{33}$$

Equation (34) includes terms to account for the effects of mass-transfer blocking in the boundary layer

$$\dot{w} = 9.34 \times 10^{-4} \rho_\infty{}^{0.661} u_\infty{}^{0.840} \{[1.0 + 3.03 \times 10^{-8} u_\infty{}^2]^{1/4} - 1.0\} \tag{34}$$

Table 2 summarizes the coolant wastage that results for the three equations.

Table 2 Flow-control equation coolant wastage

	Wastage (%)				
Equation	Traj 1	Traj 2	Traj 3	Traj 4	Traj 5
32	11.31	11.32	3.75	11.31	11.91
33	53.40	31.36	58.66	30.55	27.74
34	32.64	28.00	20.90	27.74	15.60

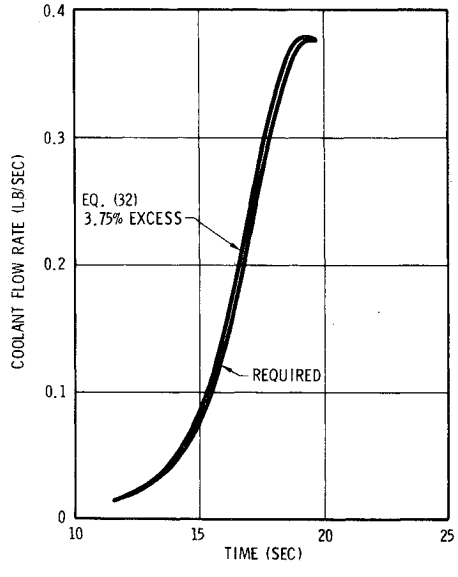

Fig. 13 Coolant flow history—Trajectory 3.

Derivation of Freestream Parameters

Equation (32) requires freestream density, velocity, and angle of attack in order to define coolant flow rate. These parameters can be readily evaluated from acceleration measurements on the three vehicle axes.

Angle of Attack

In general terms, the normal and axial acceleration due to aerodynamic forces on a re-entry vehicle are

$$\eta_N = \rho_\infty u_\infty{}^2 A_B C_N / M \tag{35}$$

and

$$\eta_Z = \rho_\infty u_\infty{}^2 A_B C_Z / M \tag{36}$$

while the normal acceleration is the resultant of that on two axes

$$\eta_N = (\eta_x{}^2 + \eta_y{}^2)^{1/2} \tag{37}$$

The normal drag coefficient is a first-order function of angle of attack, and the axial drag coefficient can be represented as a second-order function of angle of attack

$$C_N = K_4 \alpha \tag{38}$$

$$C_Z = K_5 + K_6 \alpha + K_7 \alpha^2 \tag{39}$$

By taking the ratio of the normal and axial accelerations, Eqs. (35–39) can be solved for the vehicle angle of attack

$$|\alpha| = 0.5\left(\frac{C_2}{\xi_N} - C_1\right) \pm \left[0.25\left(C_1 - \frac{C_2}{\xi_N}\right)^2 - C_3\right]^{1/2} \tag{40}$$

where ξ_N is the ratio of normal to axial acceleration

$$\xi_N = \eta_N / \eta_Z \tag{41}$$

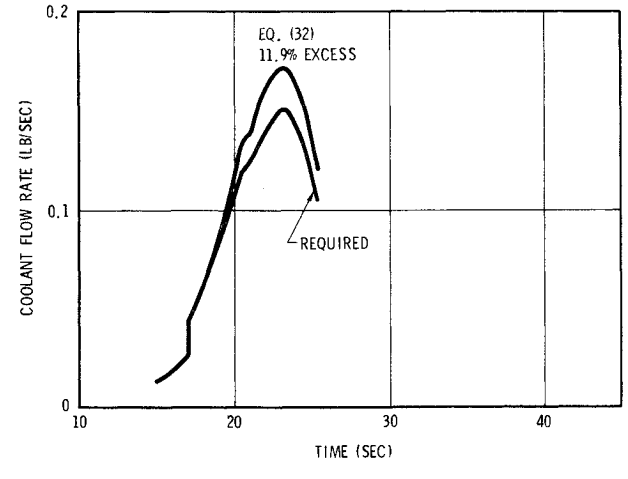

Fig. 15 Coolant flow history—Trajectory 5.

and

$$C_1 = K_6/K_7; \qquad C_2 = K_4/K_7; \qquad C_3 = K_5/K_7 \tag{42}$$

Freestream Velocity

The vehicle accelerations on body axes can be resolved into a coordinate system based on the vehicle flight path or freestream velocity vector. Two components result: a drag component parallel to the freestream vector and a lift component perpendicular to the freestream vector

$$\eta_D = \eta_Z \cos\alpha + \eta_N \sin\alpha \tag{43}$$

$$\eta_L = \eta_Z \sin\alpha + \eta_N \cos\alpha \tag{44}$$

Vehicle velocity can be well approximated by integrating the drag acceleration

$$u_{\infty,b} = u_{\infty,a} + \int_{t_a}^{t_b} (\eta_Z \cos\alpha + \eta_N \sin\alpha)\, dt \tag{45}$$

Freestream Density

Freestream density can be approximated in several ways. It can be derived from the dynamic pressure and freestream velocity

$$\rho_\infty = (q/u_\infty{}^2) g_c \tag{46}$$

It can be derived from the freestream velocity and axial deceleration

$$\rho_\infty = (M/A_B)(\eta_Z/u_\infty{}^2 C_Z) \tag{47}$$

where the axial drag coefficient, C_Z, can be defined as a function of angle of attack, as in Eq. (39). Finally, freestream density can be evaluated if vehicle altitude is known and a suitable atmospheric density model is available. Vehicle altitude can be determined from a radar altimeter or by integration of vehicle accelerations and use of a suitable coordinate transformation.

Atmospheric density is often correlated as a simple exponential function of altitude. Due to variations in temperature, however, large mismatches can occur. Up to 200,000 ft, it appears that temperature can be correlated by a third-degree polynomial, suggesting Eq. (48) for density

$$\rho_\infty = \rho_{\text{ref}} \exp(C_4 + C_5 h + C_6 h^2 + C_7 h^3) \tag{48}$$

where the reference density and altitude coefficients would be based on conditions within the expected re-entry area.

Using the form of Eq. (48) in conjunction with the ARDC 1959 atmosphere model, a least-squares fit of the natural logarithm of density with altitude has led to Eq. (49) for a density fit between sea level and 200,000 ft geometric altitude

$$\rho_\infty = 0.0752 \exp(0.0419 - 3.05\times10^{-5} h - 1.96\times10^{-10} h^2 + 7.15\times10^{-16} h^3) \tag{49}$$

The density error is within 6%.

Conclusions

The following conclusions may be made: 1) Boundary-layer heating parameters can be correlated using simple relationships involving freestream velocity, density, and local slope. 2) One-dimensional porous flow estimates provide a basis for optimizing transpiration nosetip inner contours. 3) An extension of the boundary-layer heating relationships provides a good correlation for controlling coolant flow. In order to reduce coolant wastage, the correlation must account for mass transfer and angle-of-attack effects. 4) Vehicle accelerations can be utilized to provide the parameters for the flow-control equation.

References

[1] Lee, T. G. and Mason, C. B., "Sphere/Cone Flowfield and Heat Transfer Analysis—Computer Program H586," DAC-63147, Feb. 1969, Douglas Aircraft Co., Santa Monica, Calif.

[2] Schuster, J. R., "MDAC Computer Program H859, Coolant Flow in Transpiration-Cooled Nosetips," MDC G2287, April 1971, McDonnell Douglas Astronautics Co., Huntington Beach, Calif.

[3] Van Driest, E. R., "The Problem of Aerodynamic Heating at Hypersonic Speeds," *Aeronautical Engineering Review*, Vol. 15, No. 10, Oct. 1956, pp. 26–41.

[4] Bartle, E. R. and Leadon, B. M., "The Effectiveness as a Universal Measure of Mass Transfer Cooling for a Turbulent Boundary Layer," *Proceedings of the 1962 Heat Transfer and Fluid Mechanics Institute*, University of Washington, Seattle, Wash., June 1962.

[5] Rubesin, M. W., "An Analytical Estimation of the Effect of Transpiration Cooling on the Heat-Transfer and Skin-Friction Characteristics of a Compressible Turbulent Boundary Layer," TN 3341, Dec. 1954, NACA.

[6] Arne, C. L., "Ablative Materials Subject to Combustion and Thermal Radiation Phenomena," Paper 1851, Jan. 1964, Douglas Aircraft Co., Santa Monica, Calif.